Domain Formation and Orbital Ordering Transition in a Doped Jahn-Teller Insulator

Sanjeev Kumar,[1] Arno P. Kampf,[1] and Pinaki Majumdar[2,3]

[1]*Institute of Physics, Theoretical Physics III, Center for Electronic Correlations and Magnetism, University of Augsburg,*
D-86135 Augsburg, Germany
[2]*Institut Laue-Langevin, Boîte Postale 156, 38042 Grenoble Cedex 9, France*
[3]*Harish-Chandra Research Institute, Chhatnag Road, Jhusi, Allahabad 211 019, India*

The ground state of a double-exchange model for orbitally degenerate e_g electrons with Jahn-Teller lattice coupling and weak disorder is found to be spatially inhomogeneous near half filling. Using a real-space Monte Carlo method we show that doping the half-filled orbitally ordered insulator leads to the appearance of hole-rich disordered regions in an orbitally ordered environment. The doping driven orbital order to disorder transition is accompanied by the emergence of metallic behavior. We present results on transport and optical properties along with spatial patterns for lattice distortions and charge densities, providing a basis for an overall understanding of the low-doping phase diagram of $La_{1-x}Ca_xMnO_3$.

Hole-doped perovskite manganites, for example $La_{1-x}Ca_xMnO_3$ (LCMO), are well known for their colossal magnetoresistance (CMR) effect [1,2]. The "optimally doped" CMR compounds with $x \sim 0.3$ have been the focus of numerous theoretical studies and are qualitatively understood in terms of the interplay of the double-exchange mechanism, electron-phonon interactions, and disorder in a single electronic band [3–6]. Less attention has been given to the low-doping regime, where the two-band character of manganites is crucial and in addition to charge, spin, and lattice variables, the orbital degrees of freedom and their ordering become important. The un-doped compounds are orbitally ordered (OO), *A*-type anti-ferromagnetic insulators [7] with large Jahn-Teller (JT) distortions of the MnO_6 octahedra [8], which lift the de-generacy of the two Mn-e_g levels. Electronic and coopera-tive lattice effects lead to simultaneous staggered ordering in both, the JT lattice distortions and the local orbital occupancies. Upon doping, the antiferromagnetic insulator evolves into a ferromagnetic insulator, with weakened orbital order, and eventually undergoes a transition to an orbitally disordered ferromagnetic metal (OD-FM-M) [9]. Despite the achieved progress towards an understanding of magnetic and orbital ordering in the undoped compounds [10], efforts for analyzing the doping driven transition from the orbitally ordered insulating to the orbitally disordered metallic phase have remained limited. A simple view of this transition rests on an entirely classical picture in terms of random fields introduced by the doped holes [11].

The critical hole doping x_{OD} for the loss of orbital order is close to the doping x_{IMT} for the insulator-metal transition (IMT) in LCMO, where $x_{IMT} \sim 0.22$ [12]. In lower band-width materials like $Pr_{1-x}Ca_xMnO_3$ (PCMO) the insulat-ing phase persists to even larger hole concentrations [13]. NMR and neutron scattering experiments suggest, that the doping regime $x \lesssim x_{IMT}$ is spatially inhomogeneous in LCMO with coexisting "hole poor" orbitally ordered and "hole-rich" orbitally disordered regions [14], and

the observation of confined "spin waves" confirms the existence of magnetic clusters on the nanoscale [15]. It has remained unclear how the JT insulator evolves from the homogeneous OO state at $x = 0$ to the homogeneous OD metal at optimal doping through an intermediate inhomo-geneous state.

In this Letter we present results on a two-band double-exchange model with electron-lattice coupling and disor-der in two dimensions (2D) using a real-space technique. We provide a description for the doping driven loss of orbital order and the detailed doping vs temperature phase diagram at intermediate electron-lattice coupling, appro-priate to LCMO. Results for charge transport and spectral properties are presented, which characterize the metal-insulator transitions. Real-space structures for the inhomo-geneous state of the hole-doped insulator allow us to follow the emergence of orbitally disordered domain walls and their evolution with doping.

Specifically, we consider a two-band model for itinerant e_g electrons coupled to JT lattice distortions and to local-ized $S = 3/2$ t_{2g} spins in the presence of substitutional disorder, described by the Hamiltonian:

$$H = \sum_{\langle ij \rangle \sigma}^{\alpha\beta} t_{ij}^{\alpha\beta} c_{i\alpha\sigma}^{\dagger} c_{j\beta\sigma} + \sum_i (\epsilon_i - \mu)n_i - J_H \sum_i \mathbf{S}_i \cdot \boldsymbol{\sigma}i$$
$$+ J_S \sum_{\langle ij \rangle} \mathbf{S}_i \cdot \mathbf{S}_j + \lambda \sum_i \mathbf{Q}_i \cdot \boldsymbol{\tau}_i + \frac{K}{2} \sum_i |\mathbf{Q}_i|^2. \quad (1)$$

The magnetic properties arise from the competition be-tween the Hund's rule coupling J_H driven double exchange and the antiferromagnetic superexchange J_S between the t_{2g} core spins $\mathbf{S}_i$.

In Eq. (1), c and $c^{\dagger}$ are annihilation and creation opera-tors for e_g electrons and α, β are summed over the two Mn-e_g orbitals $d_{x^2-y^2}$ and $d_{3z^2-r^2}$, which are labeled (a) and (b) in what follows. $t_{ij}^{\alpha\beta}$ are the hopping matrix ele-ments between e_g orbitals on nearest-neighbor sites and

have the cubic perovskite specific form: $t_x^{aa} = t_y^{aa} \equiv t$, $t_x^{bb} = t_y^{bb} \equiv t/3$, $t_x^{ab} = t_x^{ba} \equiv -t/\sqrt{3}$, $t_y^{ab} = t_y^{ba} \equiv t/\sqrt{3}$ [1], where x and y denote the spatial directions on a square lattice. The disorder is modeled by random on-site potentials ϵ_i, with equally probable values $\pm\Delta$. The e_g-electron spin is $\sigma_i^\mu = \sum_{\sigma\sigma'}^\alpha c_{i\alpha\sigma}^\dagger \Gamma_{\sigma\sigma'}^\mu c_{i\alpha\sigma'}$, where Γ^μ are the Pauli matrices. λ denotes the strength of the JT coupling between the distortion $\mathbf{Q}_i = (Q_{ix}, Q_{iz})$ and the orbital pseudospin $\tau_i^\mu = \sum_\sigma^{\alpha\beta} c_{i\alpha\sigma}^\dagger \Gamma_{\alpha\beta}^\mu c_{i\beta\sigma}$ [1]. K controls the lattice stiffness, and μ is the chemical potential.

We set $t = 1$ as the reference energy scale. In the manganites $J_H \gg 1$, and we adopt the frequently used limit $J_H \rightarrow \infty$, which retains the essential physics [1]. We use $J_s = 0.05$ throughout, which is estimated from the Néel temperature for $CaMnO_3$, where antiferromagnetism is purely superexchange driven. The parameters λ and Δ will be selectively explored. The spins are assumed to be classical unit vectors, $|\mathbf{S}_i| = 1$; quantum effects in the lattice variables are not considered, and the stiffness is set to $K = 1$. In the limit $J_H \rightarrow \infty$ the spin of the e_g electrons is tied to the orientation of the local core spin leading to a two-orbital "spinless" fermion model with core spin configuration dependent hopping amplitudes [1].

Replacing a fraction x of rare earth ions with 2^+ cations in the parent manganites affects the mean A-site ionic radius $r_A(x)$ as well as its variance $\sigma_A(x)$. The varying r_A modifies the electronic hopping amplitude, and hence the λ/t ratio, while σ_A controls the disorder strength Δ. In most of what follows we set $\lambda = 1.6$, which reproduces the transport gap ~ 0.4 eV (if we assume $t \sim 0.2$ eV) in $LaMnO_3$ estimated from the activated resistivity behavior [16]. We set $\Delta = 0.4$ as a typical value for weak disorder, and explore the doping and temperature dependence. Naturally the amount of disorder depends on the doping level, but this variation is not addressed here.

The model defined in Eq. (1) has been studied earlier using mean-field methods, as well as exact diagonalization (ED) based Monte Carlo (MC) simulations [17]. While the mean-field approximation excludes by construction the possible existence of inhomogeneous phases, the accessible system sizes within ED-MC simulations are too small (~ 100 sites) to explore spatial clustering effects, the orbital order to disorder transition, or the IMT itself. Here we use the traveling cluster approximation (TCA), which readily allows access to systems of ~ 1000 sites to anneal the classical spin and lattice variables. ED of the full fermionic Hamiltonian is used only for computing the electronic quantities in the TCA-generated classical configurations. This method has been benchmarked before [18] and applied to a one-band version of Eq. (1) [5].

Figure 1 summarizes our results for the OO-OD transition, magnetism, and the doping and temperature driven IMT. Panel (a) shows the $x - T$ phase diagram for $\lambda = 1.6$ and $\Delta = 0.4$. Squares mark the ferromagnetic (FM) to paramagnetic (PM) crossover and circles denote the orbital
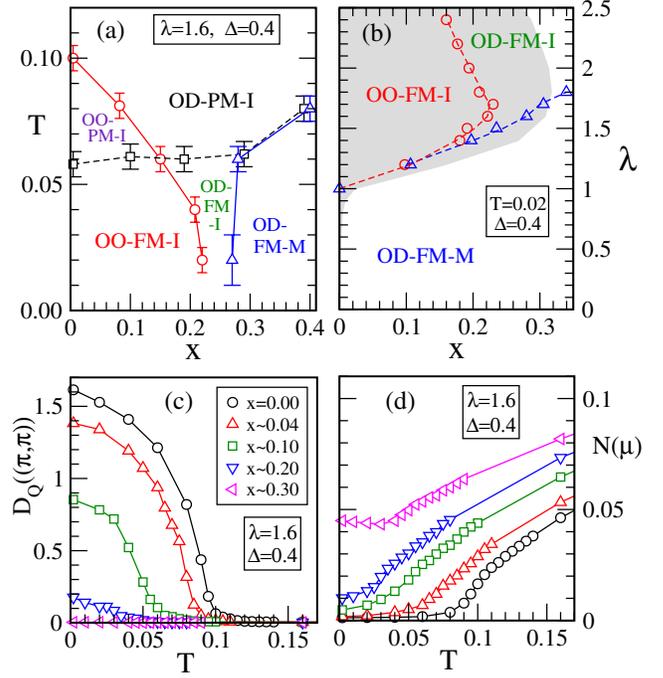
FIG. 1 (color online). (a) $x - T$ phase diagram at $\lambda = 1.6$. (b) $x - \lambda$ phase diagram at $T = 0.02$. The disorder strength is $\Delta = 0.4$. The shaded region in (b) indicates phase separation. OO (OD) refers to an orbitally ordered (disordered) phase; FM (PM) denotes a ferromagnetic (paramagnetic) state and M (I) indicates metallic (insulating) character. T dependence of (c) the lattice structure factor $D_Q(\mathbf{q}_0)$ and (d) the density of states at the chemical potential $N(\mu)$ for different x.

ordering transition temperatures T_{OO} as inferred from the T dependence of the $\mathbf{q} = (\pi, \pi) \equiv \mathbf{q}_0$ component of the lattice structure factor, $D_Q(\mathbf{q}) = N^{-2} \sum_{ij} \langle \mathbf{Q}_i \cdot \mathbf{Q}_j \rangle_{av} \times e^{-i\mathbf{q}\cdot(\mathbf{r}_i - \mathbf{r}_j)}$ shown in panel (c). Here and below $\langle...\rangle_{av}$ denotes the combined average over thermal equilibrium configurations and over the realizations of quenched disorder. The I-M boundary is obtained from the sign of the slope of the resistivity $\rho(T)$ [see Fig. 2(a)]. At $T = 0$ the system is ferromagnetic at all doping levels, despite the presence of the antiferromagnetic superexchange coupling J_S; the doping driven OO-OD transition at $x_{OD} \sim 0.22$ occurs close below the IMT. For $x < x_{OD}$ the system loses either ferromagnetic order (for $x \rightarrow 0$) or orbital order first (for x near x_{OD}) with increasing T, and for $T \gtrsim 0.1$ the system becomes an orbitally disordered paramagnetic insulator (OD-PM-I).

A broader perspective for the OO-OD transition is obtained from the low temperature $\lambda - x$ phase diagram for $\Delta = 0.4$, shown in Fig. 1(b). For our choice of J_S the system is FM over the entire selected parameter range. In the clean limit, $\Delta = 0$, the major feature is phase separation (PS), as indicated by the gray shaded area, between the OO-FM-I at $x = 0$ and the OD-FM-M for $x > 0$. PS is identified from the existence of a jump in the average hole density upon varying the chemical potential. In the pres-
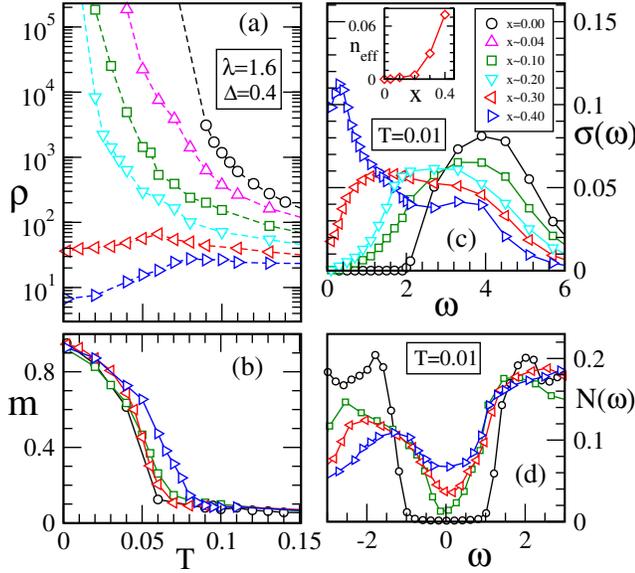
FIG. 2 (color online).   (a) Resistivity ρ on a logarithmic scale in units of $\hbar/\pi e^2$ and (b) magnetization m as a function of temperature for different x. The low temperature (c) optical conductivity $\sigma(\omega)$ and (d) density of states $N(\omega)$ for varying x. The results are for $\lambda = 1.6$ and $\Delta = 0.4$. A Lorentzian broadening of 0.02 is employed for the DOS calculations.

ence of disorder the PS range is replaced by inhomogeneous phases. We identify three distinctly different regimes with respect to λ: (i) For $\lambda \lesssim 1$ orbital ordering is absent and the system is metallic over the entire doping range. (ii) When $1 < \lambda < 1.6$ the system sustains orbital order even away from $x = 0$, and the orbital order and the insulating character is lost at a critical doping $x_{OD}(\lambda) \approx x_{IMT}(\lambda)$, which reflects that the insulating character is intimately related to the staggered ordering of the lattice distortions. (iii) For $\lambda > 1.6$ the system first loses orbital order and subsequently becomes metallic at higher doping, so $x_{IMT} > x_{OD}$. In fact, for $\lambda \gtrsim 2$ the system does not become metallic even for $x > 0.3$. This is the strong coupling regime where single electrons can be "self-trapped" and orbital ordering is not a prerequisite for the insulating behavior. If we assume that $\lambda/t \sim 1.6$ is appropriate to LCMO, the phase diagram in Fig. 1(a) agrees remarkably well with the experimental results reported in Ref. [12]. The lower bandwidth materials would correspond to larger λ/t, and indeed we find that the insulating character persists to much larger x for larger λ, consistent with the experiments on PCMO [13,19]. We remark that some aspects of the 3D manganite physics are not contained in our 2D calculation; e.g., we cannot address the crossover from an A-type antiferromagnet to a FM state; the present results should thus be compared to the physics of a single plane of the real materials only.

Figure 1(c) shows the temperature dependence of $D_Q(\mathbf{q}_0)$, which is a measure of the staggered ordering tendency of the JT distortions, for different hole concen-

trations. Since the lattice distortions are coupled to the orbital pseudospin, the same tendency is transferred to the analogously defined orbital structure factor $D_\tau(\mathbf{q}_0)$. Therefore, $D_Q(\mathbf{q}_0)$ serves as an indicator for the staggered ordering of both the lattice distortions and the orbital pseudospin. Staggered order is found only in the Q_x component of the distortions.

In the undoped case the onset of orbital order is accompanied by the opening of a gap around the Fermi level in the density of states (DOS) $N(\omega) = N^{-1}\langle\sum_n \delta(\omega - \epsilon_n\{\mathbf{Q},\mathbf{S}\})\rangle_{av}$, where $\epsilon_n\{\mathbf{Q},\mathbf{S}\}$ denote the single particle eigenvalues for a configuration $\{\mathbf{Q},\mathbf{S}\}$ of the classical variables. Figure 1(d) tracks the temperature dependence of $N(\mu)$ for the same choice of x values as in Fig. 1(c). $N(\mu)$ vanishes at low temperatures for $x \lesssim 0.10$, indicative for insulating behavior but retains a small finite value for $x \gtrsim 0.10$; the latter is in fact related to a pseudogap structure in the DOS and suggests a possibly "metallic" state (see Fig. 2).

In order to discuss the implications for transport we compute the optical conductivity $\sigma(\omega)$ using the Kubo formula with the exact eigenstates [20]. The resistivity ρ is approximated by the inverse of $\sigma(\omega_{min})$, where $\omega_{min} = 20t/N \sim 0.03t$ is the lowest reliable frequency scale for $\sigma(\omega)$ calculations on our $N = 24^2$ system. Figure 2(a) shows the temperature dependence of ρ for different x. For $x \lesssim 0.2$ there is a sharp rise in $\rho(T)$ at the onset temperature for orbital ordering T_{OO}. For $x \sim 0.3$ and $x \sim 0.4$, however, there is a downturn in $\rho(T)$ upon cooling. We correlate this behavior with the temperature dependence of the magnetization $m(T)$ defined via $m^2 = \langle(N^{-1}\sum_i \mathbf{S}_i)^2\rangle_{av}$, shown in Fig. 2(b). For all values of x a para- to ferromagnet transition is observed upon cooling, with the Curie temperature T_c inferred from the inflection point in $m(T)$. Note that T_c does not increase with increasing x, contrary to the simple double-exchange scenario [21]. Figure 2(c) shows the optical conductivity at low temperature for different x. For $x \lesssim 0.2$ the low-frequency spectral weight is strongly suppressed, which is evident in the effective carrier density $n_{eff}(\omega, x) = \int_0^\omega \sigma(\omega')d\omega'$ at $\omega = 1$, shown in the inset. For $x = 0.3$, $\sigma(\omega)$ remains finite at the lowest attainable ω, but the response is non-Drude like, while at $x = 0.4$ a more conventional optical response emerges. Nevertheless, even at $x = 0.4$, n_{eff} is strongly suppressed compared to the naive electron count. This is consistent with our observation in the disordered one-band model [5] and appears as a generic feature of the interplay of disorder and electron-lattice coupling. Figure 2(d) shows how the DOS evolves from the "clean gap" at $x = 0$ through the low x pseudogap to the high T_c "metallic" regime. The clean gap at $x = 0$, which originates from the nesting instabilities at weak coupling [22] and effective repulsions between self-trapped electrons at strong coupling, is stable in the presence of weak disorder [23]. From the combination of $N(\mu)$, $\rho(T)$, and $\sigma(\omega)$ we conclude that the electron system at $T = 0$ has an "IMT" near $x = 0.25$.
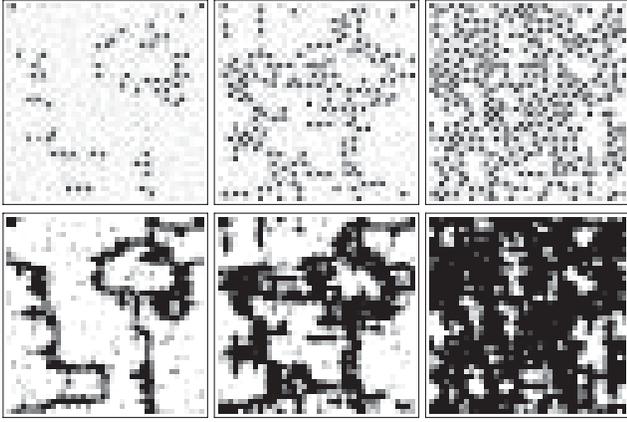
FIG. 3. Spatial patterns at $x = 0.04$, 0.11, and 0.19 (left, middle, right). Top row: charge density, grayscale covers the range from 0.2 (black) to 1 (white). Bottom row: local correlations of the lattice distortions C_Q^i. Gray scale from -1.5 (white) to 0 (black). All results are for a specific disorder realization on a 40×40 lattice, $T = 0.01$, $\lambda = 1.6$, and $\Delta = 0.4$.

For a more microscopic understanding of these results, we have examined the doping evolution of the real-space patterns for the local charge density n_i and the local spatial correlations of the lattice variables $C_Q^i = \frac{1}{4}\sum_\delta \mathbf{Q}_i \cdot \mathbf{Q}_{i+\delta}$ for a representative disorder realization, where δ is summed over the nearest neighbors of site i. The n_i in the upper row in Fig. 3 show (with white marking the hole-poor and black the hole-rich regions) that the doped holes at low x lead to a strong density variation, although the holes are not "site localized". The hole positions are spatially correlated with a short range charge order pattern. The spatial pattern is filamentary, rather than "puddle-like", with the linear structures connecting up for $x \sim x_{\mathrm{OD}}$. The C_Q^i pattern is understood from the hole locations, and the above discussed supression of $D_Q(\mathbf{q}_0)$ arises from the loss of OO in the vicinity of the holes as well as from the presence of antiphase domains separated by the hole-rich domain walls.

Although local Coulomb interactions were not explicitly included in our model analysis their effects are nevertheless partially captured. For example, the large J_H avoids double occupancy of a single orbital and therefore acts like an *intraorbital* Hubbard repulsion. The JT polaron binding energy, $\sim \lambda^2/2K$, has effects similar to an *interorbital* Hubbard repulsion since it prefers one e_g electron per site [10]. Therefore we do not expect qualitative changes in our phase diagrams if explicit electron-electron interactions were included. The T_{OO} scale however will be affected. The cooperative nature of the lattice distortion will also enhance T_{OO} as we have checked. The critical doping for the OO-OD transition, however, does not seem to be significantly affected by cooperative effects, and neither are the spatial patterns for $x \sim x_{\mathrm{OD}}$ [23].

Naturally the IMT that we observe in our 2D model with disorder is to be understood as a crossover from an insulating phase to a weakly localized (WL) phase with a finite density of states at the Fermi level. In three dimensions the gapped insulator to WL crossover is expected to become a genuine IMT.

In summary, our results on the 2D Jahn-Teller double-exchange model reveal a doping driven transition from an orbitally ordered insulator to an orbitally disordered ferromagnetic metal in agreement with the experiments on LCMO. In the orbitally disordered regime, the system undergoes a thermally driven transition from a ferromagnetic metal to a paramagnetic insulator, characteristic of the CMR materials. The intermediate inhomogeneous phase, with coexisting orbitally ordered and orbitally disordered regions, allows a natural interpretation of the neutron scattering and NMR data in LCMO [14].

[1] For overviews see, *Nanoscale Phase Separation and Colossal Magnetoresistance*, edited by E. Dagotto (Springer-Verlag, Berlin, 2002) and [2].
[2] *Colossal Magnetoresistive Oxides*, edited by T. Chatterji (Kluwer, Dordrecht, 2004).
[3] H. Röder *et al.*, Phys. Rev. Lett. **76**, 1356 (1996).
[4] J. A. Vergés *et al.*, Phys. Rev. Lett. **88**, 136401 (2002).
[5] S. Kumar and P. Majumdar, Phys. Rev. Lett. **96**, 016602 (2006).
[6] C. Sen *et al.*, Phys. Rev. B **73**, 224441 (2006).
[7] *A*-type magnetic order refers to the antiferromagnetic stacking of ferromagnetic planes.
[8] Y. Murakami *et al.*, Phys. Rev. Lett. **81**, 582 (1998).
[9] G. Biotteau *et al.*, Phys. Rev. B **64**, 104421 (2001).
[10] T. Hotta *et al.*, Phys. Rev. B **60**, R15 009 (1999).
[11] A. J. Millis, Phys. Rev. B **53**, 8434 (1996).
[12] B. B. Van Aken *et al.*, Phys. Rev. Lett. **90**, 066403 (2003).
[13] Y. Tomioka *et al.*, Phys. Rev. B **53**, R1689 (1996).
[14] G. Papavassiliou *et al.*, Phys. Rev. Lett. **91**, 147205 (2003); M. Hennion *et al.*, *ibid.* **81**, 1957 (1998).
[15] M. Hennion *et al.*, Phys. Rev. Lett. **94**, 057006 (2005).
[16] T. T. M. Palstra *et al.*, Phys. Rev. B **56**, 5104 (1997).
[17] R. Kilian and G. Khaliullin, Phys. Rev. B **60**, 13 458 (1999); S. Yunoki *et al.*, Phys. Rev. Lett. **81**, 5612 (1998).
[18] S. Kumar and P. Majumdar, Eur. Phys. J. B **50**, 571 (2006).
[19] For a comparison with larger bandwidth materials, see, e.g., A. Pimenov *et al.*, Phys. Rev. B **59**, 12 419 (1999).
[20] S. Kumar and P. Majumdar, Eur. Phys. J. B **46**, 237 (2005).
[21] M. J. Calderón and L. Brey, Phys. Rev. B **58**, 3286 (1998).
[22] D. V. Efremov and D. I. Khomskii, Phys. Rev. B **72**, 012402 (2005).
[23] S. Kumar *et al.* (unpublished).